

## Exploring lattice symmetry evolution with discontinuous phase transition by Raman scattering criteria: The single-crystalline (K, Na)NbO<sub>3</sub> model system

Anyang Cui (崔安阳),<sup>1</sup> Yan Ye (叶艳),<sup>1</sup> Limei Zheng (郑立梅),<sup>2</sup> Kai Jiang (姜凯),<sup>1</sup> Liangqing Zhu (朱亮清),<sup>1</sup> Liyan Shang (商丽燕),<sup>1</sup> Yawei Li (李亚巍),<sup>1</sup> Zhigao Hu (胡志高),<sup>1,3,4,\*</sup> and Junhao Chu (褚君浩)<sup>1,3,4</sup>

<sup>1</sup>*Department of Electronic Engineering, Technical Center for Multifunctional Magneto-Optical Spectroscopy (Shanghai), East China Normal University, Shanghai 200241, China*

<sup>2</sup>*Department of Physics, Condensed Matter Science and Technology Institute, Harbin Institute of Technology, Harbin 150080, China*

<sup>3</sup>*Collaborative Innovation Center of Extreme Optics, Shanxi University, Taiyuan, Shanxi 030006, China*

<sup>4</sup>*Shanghai Institute of Intelligent Electronics and Systems, Fudan University, Shanghai 200433, China*



(Received 11 April 2019; revised manuscript received 13 June 2019; published 2 July 2019)

We have developed the multiperspective methods for discussing phase transition and evolution of molecular vibration using unpolarized and polarized Raman scatterings. There are three scattering characteristics serving as the criteria to judge the vibrational modes, molecular symmetry, and first-order phase transition. Except for the frequency collection of one or more phonon modes, remarkably, we first demonstrate in theory that polarized Raman scattering exhibits high sensitivity on dissecting first-order phase transition, such as the symmetry breaking and discontinuity during phase transition. Experimental results confirm that temperature dependencies of peak intensity and the depolarization ratio extracted from polarized spectra present the abrupt changes associated with the discontinuity of first-order phase transition. Thermal discontinuous transformation of the (K, Na)NbO<sub>3</sub> lattice brings into physical correspondence with the molecule polarizability and order parameter of the system, i.e., spontaneous polarization, which is the first derivative of Gibbs free energy. Hence, these methods based on the scattering criteria could be broadly adapted for more extensive studies on the phase transition in condensed matter.

DOI: [10.1103/PhysRevB.100.024102](https://doi.org/10.1103/PhysRevB.100.024102)

### I. INTRODUCTION

Investigating the phase of condensed matter and constructing a phase diagram are of fundamental importance for material science. The phase-transition characteristics play a significant role in the materials' functionality and potential applications. The classic approach to define phase of matter is to calculate the order parameters of the system [1]. Taking the case of ferroelectrics, the lattice dynamics under doping or a tunable multifield can be characterized by numerous sophisticated techniques, such as x-ray diffraction [2], temperature dependence of permittivity or a piezoelectric coefficient [3], molecule spectroscopy [4–6], spectroscopic ellipsometry [7], and so on. Raman spectroscopy, as one of the molecule spectroscopies, is widely applied to precisely study the molecular symmetry, lattice defect, surface and interface properties, internal strain, chemical bond property, and dynamics [5,6,8–11]. Ferroelectric domain structures in recent years could be visualized and illustrated by a Raman scattering technique where the underlying physical mechanism responsible for this issue also attracts more attention [12–14]. Under the electromagnetic vibration of an incident laser, the excited-electron scattering from the nonsymmetric lattice serves as radiation of the electric dipole moment, which is simply proportional to the polarizability of molecular vibration [15]. The discussion

in the overwhelming majority of studies mainly focuses on examining scattering peaks with their linewidths or positions to obtain the temperature of the phase transition, polymorphic phase transition [8,16], or thermal hysteresis transition [9,17]. However, it is often overlooked that more details about phase transition can be exposed by comprehensive analysis of scattering intensity.

The polarization effect on Raman scattering is generally regarded as a complementary powerful technique for determining the molecular orientation of crystals, the anisotropy, symmetry, and molecule configuration by tuning the incident laser and probing the scattering with a fixed direction of an electric field [18–22]. In the case of polarized scattering geometry, the peak intensity and depolarization ratio indeed carry rich information of the molecular structure [19,23]. Since Lord Rayleigh made the breakthrough in 1871 to prove that the scattering intensity is inversely proportional to the wavelength of the incident laser [24], the scattering theory and the dynamics behaviors of nuclei and light-excited electrons in the quantum realm have reached great development. In past years, some experimental studies have used the concepts of scattering characteristics including phonon frequency and depolarization ratio to investigate phase transition on various kinds of ferroelectric classes, such as Pb(In, Nb)O<sub>3</sub>-Pb(Mg, Nb)O<sub>3</sub>-PbTiO<sub>3</sub>, Pb(Zn, Nb)O<sub>3</sub>-PbTiO<sub>3</sub>, Pb(Mg, Nb)O<sub>3</sub>-PbTiO<sub>3</sub>, (Na, Bi)TiO<sub>3</sub>-BaTiO<sub>3</sub>, and SrTi<sup>18</sup>O<sub>3</sub> crystals [19,25–30]. However, few studies nowadays have ever paid attention to resolving the

\*zghu@ee.ecnu.edu.cn

intensity evolution of Raman spectra and excavating the structure-related implication inside the radiant energy. An integrated theoretical and experimental illustration about the physical correlation between molecular phase transition and polarized scattering characters still is ambiguous to date. It might be ascribed to the limited understanding on the intrinsic physical correlation between the scattering intensity and the structure property or the experience on analyzing the polarized scattering spectra. In fact, it exhibits high sensitivity for investigating the phase transition through the polarized Raman spectra and the scattering intensity. Therefore, it is desirable to specify how to understand the scattering intensity and apply different polarized scattering geometries to figure out more structural details via theoretical and experimental discussions.

The emerging alkali niobate-based ferroelectric class drew great concerns recently, depending on its environment-friendly composition and giant electromechanical performance [31,32]. The dopants ( $\text{Li}^+$  and  $\text{Ta}^{5+}$ ) in  $(\text{K}, \text{Na})\text{NbO}_3$  (KNN) compounds have been considered as a positive modification benefiting from the property enhancement [31,33,34]. The present paper systematically studies thermal-induced first-order phase transition and the lattice symmetry in the model samples, the  $\text{Li}^+$ - and  $\text{Ta}^{5+}$ -doping KNN (KNNTL) single crystals by unpolarized and polarized Raman spectroscopies. Three scattering criteria (phonon frequency, polarized scattering intensity, and depolarization ratio) are proven to be the powerful fingerprints to determine the phase of matter and the property of molecular vibration in theory. Remarkably, the physical correlation between the molecular structure and these scattering criteria has been clearly specified. Simultaneously, thermal evolution results of the scattering criteria collected from temperature-dependent unpolarized Raman spectra and four kinds of polarized scattering geometries [ $\bar{Z}(XX)Z$ ,  $\bar{Z}'(XX)Z'$ ,  $\bar{Z}(XY)Z$ , and  $\bar{Z}'(XY')Z'$ ] can precisely reveal the orthorhombic ( $O$ ) to tetragonal ( $T$ ) to cubic ( $C$ ) sequence phase transition. The intensity of polarized scattering is sensitive to the thermal dynamics of the structure and lattice symmetry of the  $\text{NbO}_6$  and the doping  $\text{TaO}_6$  octahedrons in KNNTL single crystals. Experimental results not only reflect the reliability of the theoretical discussion about the scattering criteria, but also further confirm the inherent discontinuity of the first-order phase transition.

The paper is structured as follows: Sec. II describes the basic information of the model samples and unpolarized/polarized Raman spectral characterization methods. This paper assesses in theory the scattering characters of phonon frequency (Sec. III A), polarized scattering intensity (Sec. III B), and the depolarization ratio (Sec. III C), all regarded as the significant criteria of symmetry evolution and first-order phase transition. Section III D gives further considerations on the correlation between the intensity criteria and the ferroelectric spontaneous polarization during first-order phase transition. In Sec. IV, three criteria of molecular symmetry and phase transition are experimentally confirmed by results of temperature-dependent scattering in unpolarized and polarized geometries. The last Sec. V summarizes the main conclusions of this paper and gives a brief outlook for the future.

## II. MATERIALS AND METHODS

Raman characterization was performed on a Jobin-Yvon LabRAM HR 800 micro-Raman spectrometer with a Linkam THMSE 600 heating/cooling stage in the range of 103–593 K with a heating/cooling rate of 10 K/min and a temperature accuracy of  $\pm 0.1$  K. The spectral resolution is better than  $1 \text{ cm}^{-1}$ . A laser with the wavelength of 488 nm was used as the excitation. The heating effect induced by the laser beam can be ignored because the low power of about 4 mW focused on the sample. In terms of polarized scattering, the polarizers have been placed in the excitation and detection path to define the paralleled-polarized (VV) and the crossed-polarized (VH) scattering geometries. All as-measured spectra were reduced by  $n(\omega, T) + 1$  to facilitate comparison and eliminate the contribution from the Bose-Einstein temperature factor, where  $n(\omega, T) = \frac{1}{\exp(\hbar\omega/kT) - 1}$  represents the Bose-Einstein phonon distribution, where  $\hbar$ ,  $\omega$ ,  $k$ , and  $T$  are the reduced Planck constant, phonon wave number, Boltzmann constant, and temperature, respectively.

We chose KNNTL single crystals in this paper. The  $(001)_C$ - and  $(011)_C$ -cut single crystals of standard stoichiometric composition,  $[(\text{K}_{0.8}\text{Na}_{0.2})_{0.94}\text{Li}_{0.06}]\text{Nb}_{0.85}\text{Ta}_{0.15}\text{O}_3$ , abbreviated as  $001\text{-KNNTL}$  and  $011\text{-KNNTL}$ , respectively, were synthesized by using the top-seeded solution growth method [3]. The raw materials including  $\text{K}_2\text{CO}_3$ ,  $\text{Li}_2\text{CO}_3$ ,  $\text{Na}_2\text{CO}_3$ ,  $\text{Nb}_2\text{O}_5$ , and  $\text{Ta}_2\text{O}_5$  powders of 99.99% purity were mixed and ball milled in alcohol for 12 h. Perovskite polycrystalline compounds were prepared by pressing the milled powders into pellets to be calcined at  $880^\circ\text{C}$ . Then, the mixture was melted in a Pt crucible at  $1160^\circ\text{C}$  in air. The crystals were grown by the fixed-oriented seed with a rotational speed of 6–10 rpm and a pulling rate of about 0.5 mm/h. The KNNTL crystals can be obtained after the separation from the melt surface and cooling procedures. To eliminate the surface overlayer artifacts during Raman scattering measurements,  $(001)_C$ - and  $(011)_C$ -cut KNNTL single crystals were mechanically polished.

## III. THEORETICAL ASSESSMENTS: SCATTERING CRITERIA OF FIRST-ORDER PHASE TRANSITION

Details of lattice structure evolution would be achieved by digging the molecular vibrations and phonon behavior with the variation of temperature, pressure, electric, or magnetic field [19,35–38]. Temperature dependence of structural and vibrational characteristics is taken as the instance to thoroughly discuss the first-order phase transition by Raman spectroscopy. Phonon behavior could be specified and quantified by fitting the scattering peaks according to the damped harmonic oscillator (DHO) model. Here, three scattering criteria have been illustrated as follows.

### A. Phonon frequency shift

Frequency shift of the scattering peak position is regarded as one criterion to estimate the structure transformation. As we know, the shift of phonon frequency would be derived from the phase transition of the lattice. The different molecular structure after the phase transition leads to the thorough change in the atomic arrangement, lattice symmetry, and some

basic parameters of system, such as spontaneous polarization in ferroelectric matter. Besides, temperature dependence of phonon frequency is partially derived from the anharmonicity of the potential acting on atoms in lattice. Both the phonon-phonon interaction and thermally induced deformation of a lattice contribute to the frequency shift with temperature at the constant pressure ( $P$ ) [39] as given by

$$\left(\frac{\partial \nu}{\partial T}\right)_P = \left(\frac{\partial \nu}{\partial T}\right)_V + \left(\frac{\partial \nu}{\partial V}\right)_T \left(\frac{\partial V}{\partial T}\right)_P, \quad (1)$$

where  $V$  is the crystal volume. The first part on the right of the above equation reflects an anharmonic coupling at a constant volume, whereas the second one describes the thermal expansion as harmonic. The contributions of harmonic and anharmonic components rely on the property of chemical bonds in a molecular crystal [39–41]. The explicit anharmonic interaction is used to quantify the change in vibrational amplitudes, such as the phonon occupation numbers. The implicit component of the harmonic one could quantify the change in equilibrium interatomic spacing by thermal expansion of the lattice. The volume-dilatation-driven contribution is proportional to the measured pressure coefficient. In terms of the covalent solid solutions, the values of  $d\nu/dP$ , the thermal expansivity, and the compressibility are generally positive in order that the thermal expansion-driven contribution is negative. Likewise, the phonon-occupation-driven effect also keeps the  $\left(\frac{\partial \nu}{\partial T}\right)_V$  value negative as the total coefficient  $d\nu/dT$  is [40].

Frequency evolution of a vibrational mode is usually collected on the unpolarized and polarized Raman scattering spectroscopy. Temperature dependence of phonon frequency at the phase-transition point is possibly linear discontinuous or linearly discontinuous where both could be efficiently applied to determine first- and second-order phase transition [8,9,42,43]. However, it could not distinguish the type of phase transition by phonon frequency shift. Phase-transition-driven shift of vibrational frequency is actually based on a qualitative analysis and is difficult to be quantified into a fundamental characteristic associating solely with the first-order phase transition.

### B. Evolution of polarized scattering intensity

Phase of matter is inherently defined by the geometric configuration of atoms, whose electron behavior under the light field influences is tightly related to the molecular structure, such as the symmetry and vibration details. The Born-Oppenheimer approximation illuminates that the motion of atomic nuclei and electrons in a molecule can be separated as the wave function represented by  $\Psi_{\text{molecule}} = \psi_{\text{electron}} \otimes \psi_{\text{nuclear}}$ . Under the irradiation of incident light, electrons are excited to the excited state, but the nuclei are almost free of the excitation. The excited electron can, in turn, contribute to the light radiation  $\mu_i = \mu_i^0 \cos \omega t$ . When the excited electrons return to the ground state, this process is defined as Rayleigh scattering. Raman scattering concerning the interaction between the excited electron and the nuclei may contribute to the energy exchange of the system, further reducing or amplifying the energy from the incident light. The motion of nuclei under the electric field of incident light  $\varepsilon_i = \varepsilon_0 e^{i\omega t}$  could be

presented at the normal coordinate ( $Q_k$ ) with respect to the vibrational frequency  $\omega_k$ , which follows  $Q_k = Q_k^0 \cos \omega_k t = \frac{1}{2} Q_k^0 (e^{i\omega_k t} + e^{-i\omega_k t})$ , where the  $Q_k^0$  is the coordinate of the equilibrium position [44].

For the aspheric molecules, such as ferroelectric ABO<sub>3</sub>, the excited dipole moments  $\mu_i^{\text{ext}}$  are not parallel to the direction of the electrical-field  $\varepsilon_i$  of light but are a second-order tensor of

$$\mu^{\text{ext}} = \begin{bmatrix} \mu_x \\ \mu_y \\ \mu_z \end{bmatrix} = \begin{bmatrix} \alpha_{xx} & \alpha_{xy} & \alpha_{xz} \\ \alpha_{yx} & \alpha_{yy} & \alpha_{yz} \\ \alpha_{zx} & \alpha_{zy} & \alpha_{zz} \end{bmatrix} \begin{bmatrix} \varepsilon_x \\ \varepsilon_y \\ \varepsilon_z \end{bmatrix}, \quad (2)$$

where  $\alpha_{ij}$  (C m<sup>2</sup> V<sup>-1</sup>) is the polarizability used to describe the polarization of a vibrational molecule. Polarizability  $\alpha_{ij}$  as the function of the coordinate displacement of nuclei  $\left(\frac{\partial \alpha_{ij}}{\partial Q_k}\right)$  represents the dynamical interaction in a bound system of a lattice to the external field of light and further reflects the molecular symmetry [15]. Furthermore, the excited-state dipole moment under the incident electrical-field  $\varepsilon_i$  can be given by

$$\begin{aligned} \mu_i &= \alpha_{ij} \varepsilon_i \\ &= \alpha_{ij}^0 \varepsilon_0 e^{i\omega t} + \frac{1}{2} \sum_k \left(\frac{\partial \alpha_{ij}}{\partial Q_k}\right)_0 Q_k^0 \varepsilon_0 [e^{i(\omega+\omega_k)t} + e^{i(\omega-\omega_k)t}]. \end{aligned} \quad (3)$$

In Eq. (3), the first term on the right represents Rayleigh scattering, whereas the second one corresponds to the Stokes ( $\omega - \omega_k$ ) and anti-Stokes ( $\omega + \omega_k$ ) lines, respectively. The intensity of Raman scattering is given by calculating the differential scattering cross-section  $\frac{\partial^2 \sigma}{\partial \Omega \partial \varepsilon}$ , which could be expanded in the normal coordinate of the dipole moment,

$$I_k = \frac{\partial^2 \sigma}{\partial \Omega \partial \varepsilon} = \left[ \frac{\langle Q_k^0 \rangle (\omega \mp \omega_k)^4}{32\pi c^3} \sin^2 \phi \right] |\mu_i|^2. \quad (4)$$

It is noted that the intensity is proportional to the fourth power of the scattering frequency. Therefore, in the case of the linear polarized light with a fixed direction of electric field, the radiant energy  $I(\nu)$  perpendicular to the dipole moment can be simply approximated as

$$I(\nu) \propto \frac{2\pi^3 \nu^4}{c^3} (\mu_i^0)^2, \quad (5)$$

where  $c$  is the velocity of light in vacuum. The incident energy is given by  $I_0 \propto \frac{c}{8\pi} \varepsilon_F^2$ , where  $\varepsilon_F$  is the electric field of incident light with its direction along the  $F$  axis. The electric dipole moment  $\mu_{F'}^0$  is excited by the electric field of  $\varepsilon_F$  as  $\mu_{F'}^0 = \alpha_{F'F} \varepsilon_F$ . The scattering intensity could be expressed by

$$I \propto \frac{2\pi^3 \nu^4}{c^3} (\alpha_{F'F} \varepsilon_F)^2 = \frac{16\pi^4 \nu^4}{c^4} \alpha_{F'F}^2 I_0. \quad (6)$$

When the electric field of scattering and incident light is in the same direction ( $F' = F$ ), the scattering intensity follows  $I_{F'=F} \propto \alpha_{FF}^2$ . Therefore, it has demonstrated in theory that the polarized scattering intensity is proportional to the polarizability. The classic hypothesis [44] from Wolkenstein proposed that the polarizability could be defined as  $\alpha_{F'F} = \Sigma \alpha_l + \Sigma \alpha_a$ , where  $\alpha_l$  is the bond polarizability reflecting the

property of the chemical bond, such as the bond polarity, as well as  $\alpha_a$  is the atomic polarizability revealing the atomic displacement polarization, respectively. Therefore, the above discussion clarifies that the polarized scattering intensity could be considered as an important criterion to judge the structure transformation of a molecule.

### C. Evolution of the depolarization ratio

Last but not least, structural symmetry and vibration configuration could be estimated by calculating the ratio of peak intensity between the orthogonal-polarized scattering geometries. The depolarization ratio ( $\rho_l$ ), as a powerful index, is usually used to study the polarized scattering spectra. It could be regarded as the third criterion for indicating the symmetry evolution and phase transition. The value of  $\rho_l$  can be figured out by

$$\rho_l = \frac{I_{VH}}{I_{VV}} = \frac{3\beta^2}{45\bar{\alpha} + 4\beta^2}, \quad (7)$$

where  $\bar{\alpha}$  is the average of polarizability along three primary crystallographic axes and  $\beta^2$  presents the degree of anisotropy [15,23]. The depolarization ratio represents the degree to which the electrical field of incident light is twisted from the  $X$  to the  $Y$  direction. This twist behavior is ascribed to the non-spherically symmetric polarizability. In other words, the measured molecule is not a spherically symmetric structure if  $\rho_l \neq 0$ . Thus, it serves as a powerful parameter to judge the molecular geometry by the value of the depolarization ratio and investigate the structural transformation.

The first criterion about the phonon frequency can be basically obtained from both unpolarized and polarized Raman spectroscopies, whereas the criteria of scattering intensity and the depolarization ratio are only achieved by polarized Raman scattering. In the section of experimental results, the application of three scattering criteria for studying phase transition, molecular vibrations, and the lattice symmetry in KNNTL single crystals has been highlighted.

### D. Correlation between the intensity criteria and the ferroelectric spontaneous polarization during first-order phase transition

When temperature is regarded as the independent variable, the system energy is described by Gibbs free-energy ( $G_1$ ) as  $dG_1 = -S dT - x_i dx_i + E_m dD_m$ . Spontaneous polarization ( $P_S$ ) is basically considered as the order parameter to demonstrate ferroelectric phase transition [45,46] where  $P_S$  is represented by the electric displacement  $D$  as  $D = \varepsilon_0 E + P_s$  ( $E$  is the electric field, and  $\varepsilon_0$  is the permittivity). Entropy  $S$  and the electric displacement  $D$  are essentially the first derivative of Gibbs free energy with respect to the temperature and external field  $S = -(\frac{\partial G_1}{\partial T})_{x,D}$  and  $D = -(\frac{\partial G_1}{\partial E})_{x,S}$ , respectively, where the second-order tensor  $x_i$  is the constant strain of the system [45]. Hence, first-order phase transition defines spontaneous polarization of the system as the first derivative of Gibbs free energy to be discontinuous [45].

Spontaneous polarization ( $P_S$ ) directly contributes to the macroscopic distribution of the ferroelectric domain structure. As aforementioned, scattering criteria in the above sections

III B and III C, the polarized scattering intensity and the depolarization ratio could be used to figure out the structural transformation and symmetry evolution. Meanwhile, the change in the ferroelectric domain during thermal phase transition would be considered in the temperature dependence of polarized scattering intensity and the corresponding intensity ratio. It has been proven in Eq. (6) that the polarized scattering intensity is proportional to the polarizability ( $\alpha_{FF}$ ) of the dynamical interaction with respect to the normal coordinate  $Q_k$  in a bound lattice system. In this case, the dynamic system represented by polarizability on a local range is associated with the influences of local stress ( $s$ ) and/or electric-field ( $E_k$ ) given by

$$\frac{d\alpha_{ij}}{dQ_k} = \frac{d\tilde{\alpha}_{ij}}{dQ_k} + \left( \frac{\partial\alpha_{ij}}{\partial s_{lm}} ds_{lm} + \frac{\partial\alpha_{ij}}{\partial E_k} dE_k \right) \frac{1}{dQ_k}, \quad (8)$$

where  $\tilde{\alpha}_{ij}$  is the polarizability at uniform stress and field [12,14]. The derivative value of the polarizability for any first-order phonon is, in principle, expected to diminish in a multidomain material, and thus, it has to decrease near the domain walls because of the increasing disorder in the lattice caused by cell parameters mismatch and distortions. The spontaneous polarization contribution, originated from the first derivative of energy, has been involved in the polarizability dynamics. In other words, according to Eqs. (6) and (8), thermal evolution of polarized scattering intensity takes the existence and change in polarization and inherent strain into account and reflects the total contributions from them and intrinsic polarizability  $\tilde{\alpha}_{ij}$  during first-order phase transition. Based on this underlying mechanism, Fontana *et al.* [12] and Rüsing *et al.* [14] have confirmed that Raman scattering is capable of visualizing ferroelectric domain structures, especially a domain wall separating various polarization orientations. However, we think that it may be difficult to distinguish and quantify the contributions of three terms of Eq. (8) by exploring the Raman spectrum.

## IV. RESULTS AND DISCUSSION

### A. Temperature dependence of phonon frequency and phase transition

As addressed, phase transition may contribute to the abnormal shift of phonon frequency, which is generally used in numerous studies to serve as the criterion to determine the temperature of the phase transition. Figure 1(a) shows the unpolarized Raman spectra measured on the 001-KNNTL single crystal at the temperature range of 103–593 K. According to the group-theoretical prediction, the KNN lattice follows the space-group  $Amm2$  ( $C_{2v}^{14}$ ) with Raman-active optical modes of  $4A_1 + 4B_1 + 3B_2 + A_2$ . Both ferroelectric LiNbO<sub>3</sub> and LiTaO<sub>3</sub> compounds with the space-group  $R3c$  ( $C_{3v}^6$ ) and point-group symmetry  $3m$  yields  $4A_1 + 5A_2 + 9E$  optical modes. The scattering peaks are mainly excited at below 300, 500–650, and near 850  $\text{cm}^{-1}$ , respectively. In order to specify the phonon frequency and its thermal evolution, the Lorentzian-shaped deconvolution of the spectra is presented by the DHO model. It is generally accepted that the NbO<sub>6</sub> octahedron in the KNN lattice contains the phonon vibrations of symmetric stretching mode  $A_{1g}(\nu_1)$ , asymmetric stretching

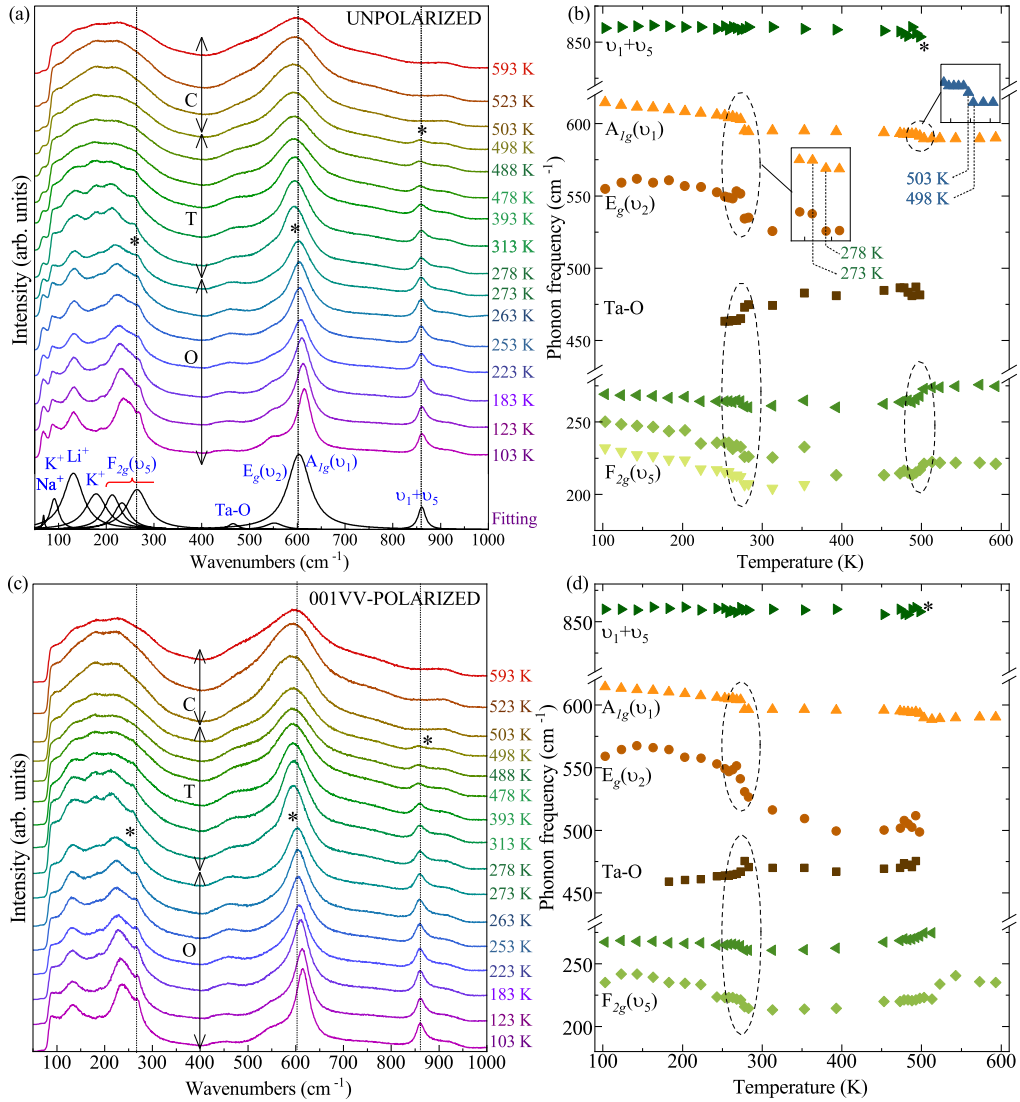


FIG. 1. (a) Unpolarized Raman spectra of the 001-KNNTL single crystal at the increasing temperatures from 103 to 593 K. The multi-Lorentz peak fitting at the bottom corresponds to the various modes of lattice vibration at 273 K. (b) The phonon frequency for the main vibrations as a function of temperature. The inset and the dashed ellipses highlight the obvious shift of the frequency. (c) Polarized Raman spectra in the parallel-polarized geometry on the 001-KNNTL single crystal at 103–593 K. (d) Temperature dependence of phonon frequency collected from the polarized scattering spectra.

modes  $E_g(\nu_2)$  and  $F_{1u}(\nu_3)$ , asymmetric bending mode  $F_{1u}(\nu_4)$ , symmetric bending mode  $F_{2g}(\nu_5)$ , and the inactive bending mode  $F_{2u}(\nu_6)$  where  $F_{1u}(\nu_3)$  and  $F_{1u}(\nu_4)$  are solely the infrared active modes. The relatively strong scattering peaks near 250 and 600 cm<sup>-1</sup>, corresponding to the  $A_{1g}(\nu_1)$  and  $F_{2g}(\nu_5)$  modes, respectively, reflect the near-perfect equilateral octahedral symmetry believed to be the space group of  $C_{2v}^{14}$  in the KNN lattice [10]. The wide overlapping peaks at 50–300 cm<sup>-1</sup> are derived from the molecular vibrations among the translational modes of the  $A$ -site cations and the  $F_{2g}(\nu_5)$  mode of the  $\text{NbO}_6$  octahedron in the KNNTL crystals. The breathing mode of  $F_{2g}(\nu_5)$  at 200–300 cm<sup>-1</sup> could be distinguished from the translational modes of  $\text{K}^+$ ,  $\text{Na}^+$ , and  $\text{Li}^+$  at the frequency range of lower than 200 cm<sup>-1</sup>. The impurity of  $\text{Ta}^{5+}$  would excite a weak scattering peak at around 450 cm<sup>-1</sup> associating with the stretching vibration of the Ta-O

bond. The peak near 860 cm<sup>-1</sup> reflects the vibrational mode of  $\nu_1 + \nu_5$  ( $A_{1g} \times F_{2g} = F_{2g}$ ).

After the identification of the lattice vibration modes according to the fitting process, we first highlighted the temperature-dependent phonon frequency involving  $\nu_1$ ,  $\nu_2$ ,  $\nu_5$ ,  $\nu_1 + \nu_5$ , and the stretching vibration of the Ta-O bond in the 001-KNNTL molecule as plotted into Fig. 1(b). The extremely weak peak at the vicinity of 450 cm<sup>-1</sup> from the Ta-O bond was only collected at the temperature range of 253–498 K. Phonon frequencies of the  $\text{BO}_6$  octahedron, except for the mode of  $\nu_1 + \nu_5$ , exhibit a slight redshift at 103–273 K. These weak redshifts of intermolecular oscillation frequencies with the temperature increasing to 273 K theoretically follow  $(\frac{\partial \nu}{\partial T})_P$  of Eq. (1) where the negative-correlated contributions could be originated from both the phonon-occupation-driven and the thermal-expansion-driven

couplings in the lattice. When the temperature increases from 273 to 278 K, the phonon frequencies of  $\nu_1$ ,  $\nu_2$ , and  $\nu_5$  present a skip redshift as marked by the dashed circles and inset in Fig. 1(b), which cannot only be explained by the effect of thermal expansion. Similarly, the phonon frequency of  $\nu_1$  shifts abruptly to a low value with the temperature rising from 498 to 503 K. The vibration of the Ta-O bonds at 273–278 K, the  $\nu_2$  and  $\nu_5$  modes at 498–503 K present the discontinuous increasing in frequency, corresponding to the blueshift of phonon frequency. The anomalies of frequency shift could fundamentally be related to the thermally induced phase transition, which is accompanied with symmetry rearrangement and the reassignment of the symmetry operation after the phase transition. In this case, the molecular distortion in a new phase structure would excite the light radiation (scattering) from the electron associating with the reassignment of the optical phonon. Therefore, the phonon frequency shift could be regarded as the typical characteristics of phase transition where the temperature of phase transformation from the O to the T phase in the KNNTL crystal lattice is 278 K and the Curie point ( $T_c$ ) is 503 K, respectively.

Meanwhile, it can be noted that phase transition is determined by the shift of phonon frequency collected by the polarized scattering spectra as well. Figures 1(c) and 1(d) show the VV scattering spectra and temperature dependence of phonon frequency on the 001-KNNTL single crystal at 103–593 K. Results present the almost identical evolution of the polarized scattering peak and peak position. The polarized scattering is only different from the unpolarized one in the electric-field direction of incident and scattering light. Hence, if a Raman-active mode can be detected by both the polarized and the unpolarized scattering geometries, the phonon frequency for a vibration mode should be not different between the polarized and the unpolarized scattering geometries. Besides, it can be seen that some phonon frequencies at the high temperatures cannot be extracted by the fitting process. High symmetry of the lattice corresponds to the broadening peaks, which results in the poor fitting for the mode with the weak peak. Some vibration modes annihilate at the highly symmetric phase, for example, the peak corresponding to the mode of  $\nu_1 + \nu_5$  disappears when the temperature is over the Curie point of 503 K.

## B. Discontinuous characteristics of first-order phase transition and polarized Raman scattering

It is generally accepted that the successive phase ( $C$ - $T$ - $O$ ) transition of KNN-based crystals belongs to first-order phase transition [17]. As the distinctive features of first-order phase transition, thermal hysteresis of the KNN system has been observed experimentally by Raman spectroscopy in our previous study [9]. Although the phonon frequency presents the skip shift, it cannot illustrate that the type of phase transition of the KNNTL single crystal is first-order discontinuous phase transition. First-order phase transition is associated with the discontinuity of the first derivative ( $\partial G_1$ ). In terms of spontaneous polarization, the intrinsic ferroelectric domain structure has to rearrange with the  $O$ - $T$  phase transition where the direction of spontaneous polarization changes from one of the face diagonals in the pseudocubic structures to one of the

cube edges in the  $T$  phase. We have revealed that the thermal evolution of spontaneous polarization in the Li-doping KNN single crystal is discontinuous during the  $O$ - $T$  phase transition by temperature-dependent out-of-plane and in-plane domain characterizations [9]. According to Eq. (8) in Sec. III D, temperature dependence of polarized scattering intensity during the first-order phase transition takes the discontinuous evolution of spontaneous polarization involved in the polarizability dynamics into account. In addition, in terms of the crystallographic symmetry, the symmetry elements among  $O$ ,  $T$ , and  $C$  phases are definitive and independent of one another where each symmetry element forms or annihilates after phase transition. The symmetry breaking during phase transition is derived from the thermally induced displacement of off-centered atoms from the highly symmetric sites. Therefore, the discontinuous phase transition can only correspond to the abrupt change in the lattice symmetry. We have theoretically clarified above that the polarized scattering provides more criteria on determining the lattice distortion and the symmetry of the Raman-active vibrations.

Polarized scattering is able to control the propagation ( $\mathbf{k}_i$ ,  $\mathbf{k}_s$ ) and electrical-field ( $\mathbf{E}_i$ ,  $\mathbf{E}_s$ ) directions of the incident and scattered light. Porto's notation [47]  $\mathbf{k}_i(\mathbf{E}_i, \mathbf{E}_s)\mathbf{k}_s$  is used to express the orientation of the crystal with respect to the polarization of the laser in both the exciting and the analyzing directions. Raman spectroscopy with the backscattering geometry requires the direction relations of  $\mathbf{k}_i = -\mathbf{k}_s$ ,  $\mathbf{k}_i \perp \mathbf{E}_i$ , and  $\mathbf{k}_s \perp \mathbf{E}_s$ . We employed the backscattering geometry to record spectra in the VV and VH polarizations on the optically polished (001)- and (011)-cut KNNTL single crystals. It should be noted for analyzing polarized scattering that the crystallographic coordinate system  $\{xyz\}$  is generally different from the one of the laboratory orthogonal frame  $\{XYZ\}$ . As shown in Fig. 2(a), the axes  $X$ ,  $Y$ , and  $Z$  are parallel to the cubic [100], [010], and [001] crystallographic directions, respectively. The scattering light is collected by an analyzer, which is oriented either VV or VH to the polarization of the incident laser, corresponding to  $\bar{Z}(XX)Z$  and  $\bar{Z}(XY)Z$  geometries, respectively. In addition, the VV and VH configurations of polarized scattering on the 011-KNNTL crystal correspond to  $\bar{Z}'(XX)Z'$  and  $\bar{Z}'(XY')Z'$ , respectively.

Temperature-dependent scattering spectra involving the parallel-polarized  $\bar{Z}(XX)Z$  (001VV),  $\bar{Z}'(XX)Z'$  (011VV), cross-polarized  $\bar{Z}(XY)Z$  (001VH), and  $\bar{Z}'(XY')Z'$  (011VH) spectra have been carried out at the range of 123–503 K. For facilitating the comparison, four types of polarized spectra at 273 and 278 K have been plotted in Figs. 2(b) and 2(c) associating with  $O$  and  $T$  phases, respectively. The peaks located at 50–200  $\text{cm}^{-1}$  mainly corresponding to translational modes of  $\text{K}^+$ ,  $\text{Na}^+$ , and  $\text{Li}^+$  were sensitive to different polarized geometries. For instance, the peak near 70  $\text{cm}^{-1}$  is only active with the orthogonal configuration of polarized scattering. The vibration mode of Ta-O bonds could be observed only in  $\bar{Z}(XX)Z$  geometry. In contrast, Raman-active modes of the  $\text{BO}_6$  octahedral  $\nu_1$ ,  $\nu_2$ , and  $\nu_5$  can be observed in all polarized geometries and do not exhibit the distinct differences among the various polarizations except for the scattering intensity. The weak shift of peak position (around 600  $\text{cm}^{-1}$ ) occurs between the  $\bar{Z}(XX)Z$  and the  $\bar{Z}'(XX)Z'$  spectra, even if these spectra were measured at the

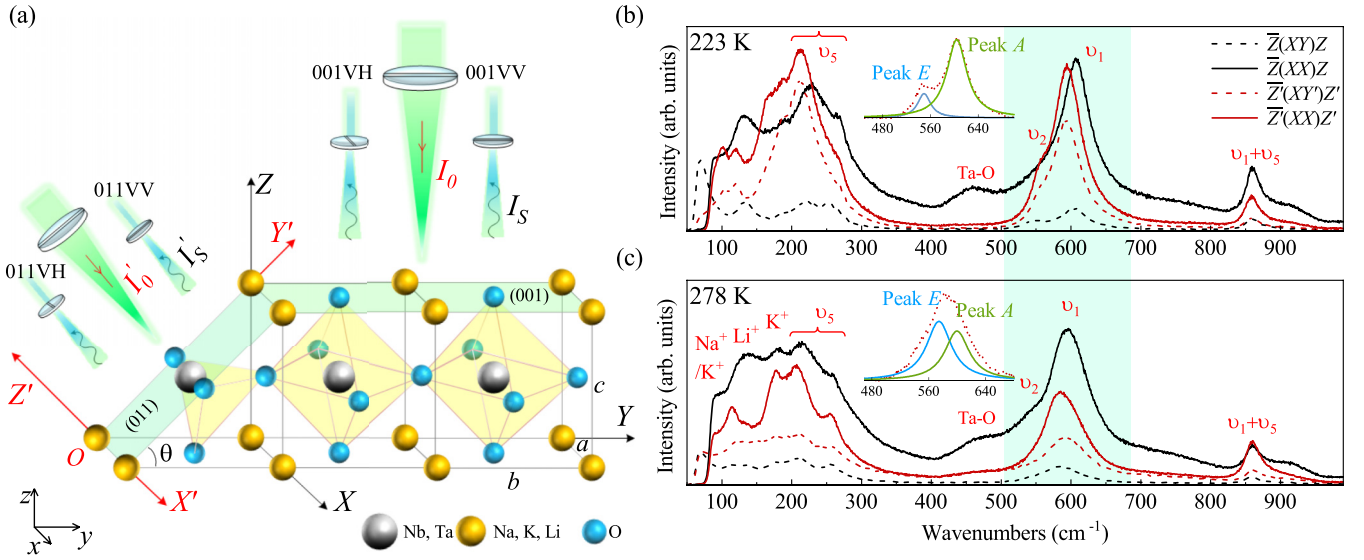


FIG. 2. (a) Schematic for polarized Raman scattering observed on the (001)-cut and (011)-cut KNNTL single crystals as an  $\text{ABO}_3$  perovskite cubic structure, respectively. The crystallographic orientation in coordinate system  $\{xyz\}$  marked in the lower-left corner follows the  $x$  axis along the  $[100]_c$  direction, the  $y$  axis along the  $[010]_c$  direction, and the  $z$  axis along the  $[001]_c$  direction, respectively. The crystallographic system  $\{xyz\}$  for the (001)-cut KNNTL crystal in this paper is considered as the same with the laboratory coordinate  $\{XYZ\}$ , whereas for the (011)-cut one, the  $\{xyz\}$  orientation differs from the laboratory frame  $\{X'Y'Z'\}$ . The polarized Raman spectra collected at (b) 223 K and (c) 278 K with the incident light polarization parallel to the cubic edge  $[\bar{Z}(XX)Z$  and  $\bar{Z}(XY)Z]$  and parallel to the cubic face diagonal  $[\bar{Z}'(XX)Z'$  and  $\bar{Z}'(XY')Z']$ . The inset indicates the Lorentzian-shaped deconvolution of the peak near  $600 \text{ cm}^{-1}$ , which is associated with the phonon modes of  $A_{1g}(\nu_1)$  marked by peak A and  $E_g(\nu_2)$  marked by peak E.

same temperature. It might be attributed to the anisotropy or the inhomogeneity of local structural distortions in the bulk crystal.

The scattering intensity of  $\bar{Z}(XY)Z$  and  $\bar{Z}(XX)Z$  configurations, respectively, could be expressed according to Eq. (6) as  $I_{\bar{Z}(XY)Z} \propto \frac{16\pi^4\nu^4}{c^4}\alpha_{YX}^2 I_0$  and  $I_{\bar{Z}(XX)Z} \propto \frac{16\pi^4\nu^4}{c^4}\alpha_{XX}^2 I_0$ . In a similar manner, owing to the same direction of the electrical field of incident light and scattering in  $\bar{Z}'(XX)Z'$  geometry, according to  $\mu_X^0 = \alpha_{XX}\varepsilon_X$ , the  $\bar{Z}'(XX)Z'$  scattering intensity meets  $I_{\bar{Z}'(XX)Z'} \propto \frac{16\pi^4\nu^4}{c^4}\alpha_{XX}^2 I_0$ . For  $\bar{Z}'(XY')Z'$  polarization, its intensity is proportional to the electric dipole moment  $\mu_{Y'}^0$ , whose vector direction along the  $Y'$  axis requires being transferred into the  $Y$  axis of laboratory coordinate where angle  $\theta$  marked in Fig. 2(a) is determined by the lattice constant of the KNNTL crystal. Hence,  $\bar{Z}'(XY')Z'$  scattering intensity could be solved as

$$\begin{aligned}
 I_{\bar{Z}'(XY')Z'} &\propto \frac{2\pi^3\nu^4}{c^3} [(\mu_{Y'}^0)^2 + (\mu_Z^0)^2] \\
 &= \frac{2\pi^3\nu^4}{c^3} [(\alpha_{YX}\varepsilon_X \cos \theta)^2 + (\alpha_{ZX}\varepsilon_X \sin \theta)^2] \\
 &= \frac{16\pi^4\nu^4}{c^4} [(\alpha_{YX} \cos \theta)^2 + (\alpha_{ZX} \sin \theta)^2] I_0. \quad (9)
 \end{aligned}$$

It has been proven in theory that the temperature dependence of scattering intensity can directly reflect the change in the polarizability of the nucleus-bound electron in the molecule. The fitting peaks [peak A and peak E in the insets of Figs. 2(b) and 2(c)] corresponding to the  $A_{1g}(\nu_1)$  and  $E_g(\nu_2)$  modes were taken as the example to discuss the thermal evolution of the normalized intensity on the 011-KNNTL

single crystal in Fig. 3(a). At the low-temperature range of 103–273 K, the intensity of the  $E_g(\nu_2)$  mode shows a mostly flat pattern for the different polarized geometries. The scattering intensity of the  $A_{1g}(\nu_1)$  mode slightly increases at first and then gradually declines, exhibiting more sensitive behavior to the external temperature. At 273 K, the scattering intensity for all polarized geometries of peaks A and E sharply goes up or down. According to the correlation between the molecular polarizability and the scattering intensity in Eqs. (6) and (9), it reflects the discontinuous dynamics of molecular polarizability at 273–278 K, corresponding to the symmetry rearrangement and breaking during the  $O$ - $T$  phase transition. With the temperature increasing from 278 to 498 K, the intensity of peaks A or E in the four types of polarized scatterings do not present the obvious change. When the temperature reaches 503 K, the steep change can be observed again. In this case, the  $T$  phase was transferred to the paraelectric  $C$  phase with high symmetry of the lattice. Therefore, the intensity evolution that could preliminarily be in accord with the discussion about the lattice symmetry evolution at the  $C$ - $T$  or  $T$ - $O$  phase transitions of the KNNTL crystals can only be discontinuous corresponding to the symmetry breaking and rearrangement in the first-order phase transition.

Moreover, it can be seen in Figs. 1(a) and 1(c) that the scattering peak of the  $\nu_1 + \nu_5$  mode near  $860 \text{ cm}^{-1}$  could clearly mark the  $T$ - $C$  phase transition at 503 K, corresponding to the peak annihilation. In order to further confirm this issue, the normalized intensity of the peak near  $860 \text{ cm}^{-1}$  collected from the polarized scattering spectra at the temperature range of 103–593 K on the 001-KNNTL and 011-KNNTL crystals has been plotted in Fig. 3(b). At the  $O$ - $T$  phase transition, the intensity in the VV scattering changes abruptly. The peak

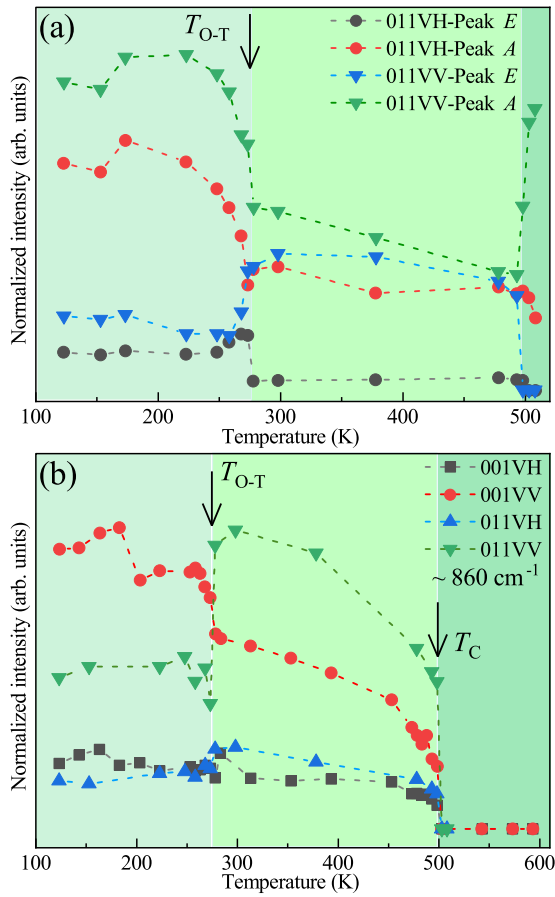


FIG. 3. Temperature-dependent normalized intensity of polarized scattering peaks corresponding to (a) the vibrations of the  $\nu_1$  mode (peak A), the  $\nu_2$  mode (peak E), and (b) the  $\nu_1 + \nu_5$  mode.

intensity declines gradually with the temperature increasing to 498 K and disappears beyond 503 K. The profiles of the radiant energy for the  $\nu_1 + \nu_5$  mode at 278 and 503 K were

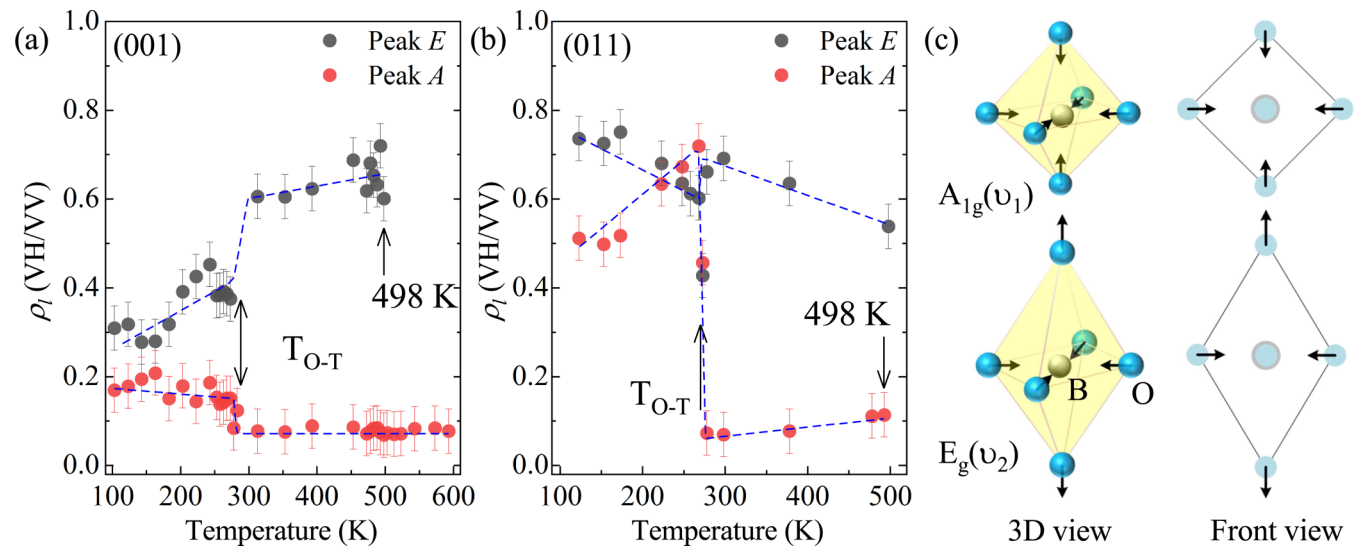


FIG. 4. Temperature dependence of the depolarization ratio ( $\rho_l$ ) observed on (a) the 001-KNNTL surface and (b) the 011-KNNTL surface. (c) Schematics [three-dimensional (3D) and the front views] of vibrations in NbO<sub>6</sub> octahedra:  $A_{1g}(\nu_1)$  (upper) and  $E_g(\nu_2)$  (lower) modes.

associated with the discontinuous dynamics of the bound electron in the asymmetric molecule, revealing that the temperature of the phase transition is 278 K ( $T_{O-T}$ ) and 503 K ( $T_C$ ), respectively. Therefore, on the basis of the theoretical and experimental analyses, temperature dependence of the peak intensity in different polarized configurations could efficiently demonstrate the lattice symmetry evolution during the  $O-T$  and  $T-C$  phase transitions.

When polarized spectra were collected on the 001-KNNTL crystal, the depolarization ratio can be calculated by  $\rho_l = \frac{I_{Z'(XY)Z'}}{I_{Z'(XX)Z'}}$ , which is proportional to the value of  $(\frac{\alpha_{YX}}{\alpha_{XX}})^2$ . For the 011-KNNTL sample, it follows  $\rho_l = \frac{I_{Z'(XY)Z'}}{I_{Z'(XX)Z'}} \propto \frac{\alpha_{XX}^2}{(\alpha_{YX} \cos \theta)^2 + (\alpha_{ZX} \sin \theta)^2}$ . Figures 4(a) and 4(b) plots the temperature-dependent depolarization ratio  $\rho_l(T)$  of peak A and peak E [the insets of Figs. 2(b) and 2(c)] on 001-KNNTL and 011-KNNTL crystals. With the temperature going up from 103 to 273 K, the ratio presents a stepwise increase in the configurations of the “001-peak E” and the “011-peak A,” or a weak decrease in the “001-peak A” and the “011-peak E.” It illustrates the continuous evolution of symmetry accompanied with thermal expansion of the lattice. The values of the depolarization ratio take a steep inclination at 273 K, corresponding to the skip changing in lattice symmetry under the phase transition.

In addition, the  $\rho_l(T)$  value for the  $A_{1g}(\nu_1)$  mode observed by peak A is generally lower than that for the  $E_g(\nu_2)$  mode. The depolarization ratio is particularly sensitive to the molecular symmetry and the configuration of the vibrational mode, e.g., tending towards the spherical or linear shape. Typically, the spherical symmetry enables the ratio to be zero due to the degree of anisotropy  $\beta^2 = 0$ . The increased value of  $\rho_l$  predicts that the molecule departs from the spherical towards the linear shape [23]. The schematics of the vibrational modes ( $\nu_1$  and  $\nu_5$ ) of NbO<sub>6</sub> octahedra can be seen in Fig. 4(c). In the KNN lattice, the vibration of  $A_{1g}(\nu_1)$  makes six oxygen atoms of BO<sub>6</sub> octahedra verge to the lattice center of the B site.

On the contrary, the  $E_g(\nu_2)$  mode would stretch the molecule along the [001] direction, leading to the more linear shape of the molecule than the  $A_{1g}(\nu_1)$  one [10]. In comparison with  $\rho_l(T)$  for the  $A_{1g}(\nu_1)$  mode, a higher ratio for the  $E_g(\nu_2)$  mode is associated with the linear-oriented vibrational configuration of the oxygen octahedron in KNNTL single crystals. In other words, the lower value of the depolarization ratio  $\rho_l$  could experimentally reflect the better spherical symmetry of the vibration mode. However, depolarization ratio  $\rho_l(T)$  calculated by  $\rho_l = \frac{I_{VH}}{I_{VV}}$  is estimated within the experimental error, which could be partially from the fitting process for the unresolvable overlap. For example, when the temperature reaches the Curie point, high symmetry of the  $C$  phase contributes to the broadening overlap peaks near 200 and 600  $\text{cm}^{-1}$ . In this case, the peak  $E$  and  $A$  modes may not be effectively separated in the highly symmetric lattice. Even so, it is an efficient approach to determine the phase transition, the symmetry evolution, and the configuration of the molecular vibration by specifying the temperature dependence of the depolarization ratio.

Therefore, the analysis on the temperature dependence of the phonon frequency, the polarized scattering intensity, and the depolarization ratio has revealed the thermally induced continuous  $O$ - $T$ - $C$  structural phase transition and discontinuous evolution of lattice symmetry in KNNTL single crystals. It also confirms the high sensitivity of polarized Raman scattering criteria on defining first-order phase transition. Moreover, we made an additional attempt to explore the successive first-order phase transitions, which generally experience from rhombohedral ( $R$ ) to  $T$  to  $C$  with temperature increasing by *in situ* polarized scattering criteria on the (001)-cut  $0.93\text{Pb}(\text{Zn}_{1/3}\text{Nb}_{2/3})\text{O}_3$ - $0.07\text{PbTiO}_3$  (PZN-PT) single crystal. Accompanied with the  $R$ - $T$  or  $T$ - $C$  phase transition, temperature dependence of polarized scattering intensity ( $I_{VH}$  and  $I_{VV}$ ) and depolarization ratio ( $\rho_l = \frac{I_{VH}}{I_{VV}}$ ) extracted at the characteristic phonon frequency, such as 780  $\text{cm}^{-1}$ , presents the anomalous change in the temperature of the phase transition. Similar experimental results could also be seen in previous important studies [19,25]. It illustrates that temperature dependence of the scattering criteria could be employed to investigate first-order phase transition in PZN-PT lattices. As a consequence, polarized Raman scattering, as one of the molecule spectroscopies in a polarized geometry, would be proven to be a powerful tool for dissecting structural evolution, phase transition, and molecular symmetry of the ferroelectric  $\text{ABO}_3$  system in detail.

## V. CONCLUSION AND OUTLOOK

This paper systematically demonstrates the multiperspective approaches on investigating the structural details, molecular symmetry, and the first-order phase transition by Raman spectroscopy, particularly, the polarized scattering. The integrated theoretical and experimental illustration about the physical correlation between first-order phase transition and

polarized scattering characters is claimed. Three central criteria have been discovered and applied to judge the first-order phase transition, symmetry evolution, and the molecular geometry. By studying the light radiation and vibration from the nuclei-bound electrons at the excited state as the representative of molecule structure and symmetry, the excited dipole moment and the molecular polarizability could be reliably reflected on the peak intensity and depolarization ratio of polarized scattering.

High-performance lead-free KNN-based ferroelectric single crystals were employed as the objects depending on their classic properties of the phase transition. Our experimental results show that temperature-dependent phonon frequency observed by depolarized Raman spectra exhibits both the continuous and the discontinuous shifts, which has been distinguished and attributed to thermally induced lattice expansion, the phonon-occupation-driven effect, and phase transition, respectively. First-order phase transition is accompanied with the discontinuous change in order parameter. Simultaneously, the symmetry property in a different phase is independent. Thus, the discontinuity of phonon dynamics is regarded as the landmark of first-order phase transition and associated with the abrupt change in molecular symmetry. Furthermore, polarized Raman scattering with cross- or parallel-polarized geometries could be better used to directly investigate the configuration of the molecular vibration mode and lattice symmetry evolution. The analysis of the depolarization ratio has revealed that the vibrational mode  $E_g(\nu_2)$  is characterized as a more linear-oriented geometry than the mode of  $A_{1g}(\nu_1)$ .

This paper provides a deeper insight into the details of the lattice structure and phase transition of the KNN system. Additionally, on the basis of the phase transition research on other typical ferroelectric classes, such as well-known  $\text{PbTiO}_3$  and  $\text{BaTiO}_3$  crystals [19,26–29], the analysis approaches considering these three scattering criteria from unpolarized and polarized Raman scatterings would be suitable to investigate first-order phase transitions and lattice symmetry evolution in more ferroelectrics. We expect to implement more investigations to verify the feasibility and study more undiscovered structure properties on more extensive condensed-matter systems.

## ACKNOWLEDGMENTS

One of the authors (A.C.) would like to thank H. Fang (Harbin Institute of Technology) for a positive discussion on the experimental results. This work was financially supported by the National Key R&D Program of China (Grants No. 2017YFA0303403 and No. 2018YFB0406500), the National Natural Science Foundation of China (Grants No. 61674057 and No. 91833303), the Projects of Science and Technology Commission of Shanghai Municipality (Grants No. 18JC1412400, No. 18YF1407200, and No. 18YF1407000), and the Program for Professor of Special Appointment (Eastern Scholar) at the Shanghai Institutions of Higher Learning.

[1] K. A. Müller, W. Berlinger, and J. C. Slonczweski, *Phys. Rev. Lett.* **25**, 734 (1970).

[2] X. Wang, J. Wu, D. Xiao, J. Zhu, X. Cheng, T. Zheng, B. Zhang, X. Lou, and X. Wang, *J. Am. Chem. Soc.* **136**, 2905 (2014).

- [3] L. Zheng, J. Wang, X. Liu, L. Yang, X. Lu, Y. Li, D. Huo, W. Lü, B. Yang, and W. Cao, *Appl. Phys. Lett.* **111**, 172903 (2017).
- [4] Z. Duan, P. Chang, Z. Hu, J. Wang, G. Wang, X. Dong, and J. Chu, *J. Appl. Phys.* **116**, 093513 (2014).
- [5] T. Xu, X. Zhao, and Y. Zhu, *J. Phys. Chem. B* **110**, 25825 (2006).
- [6] I. Lin, C. Chia, H. Liu, Y. Chen, H. Cheng, and C. Chi, *J. Eur. Ceram. Soc.* **23**, 2633 (2003).
- [7] Q. Li, J. Wang, M. Li, S. Guo, J. Zhang, Z. Hu, Z. Zhou, G. Wang, X. Dong, and J. Chu, *Phys. Rev. B* **96**, 024101 (2017).
- [8] L. Xu, K. Jiang, J. Zhang, G. Xu, Z. Hu, and J. Chu, *Appl. Phys. Lett.* **106**, 122901 (2015).
- [9] A. Cui, K. Jiang, P. Zhang, L. Xu, G. Xu, X. Chen, Z. Hu, and J. Chu, *J. Phys. Chem. C* **121**, 14322 (2017).
- [10] K. Kakimoto, K. Akao, Y. Guo, and H. Ohsato, *Jpn. J. Appl. Phys.* **44**, 7064 (2005).
- [11] R. Ratheesh, H. Sreemoolanadhan, and M. T. Sebastian, *J. Solid State Chem.* **131**, 2 (1997).
- [12] M. D. Fontana, R. Hammoum, P. Bourson, S. Margueron, and V. Y. Shur, *Ferroelectrics* **373**, 26 (2008).
- [13] G. Stone and V. Dierolf, *Opt. Lett.* **37**, 1032 (2012).
- [14] M. Rüsing, S. Neufeld, J. Brockmeier, C. Eigner, P. Mackwitz, K. Spychala, C. Silberhorn, W. G. Schmidt, G. Berth, A. Zrenner, and S. Sanna, *Phys. Rev. Mater.* **2**, 103801 (2018).
- [15] D. A. Long, *Raman Spectroscopy* (McGraw-Hill, New York, 1977).
- [16] T. Zheng, H. Wu, Y. Yuan, X. Lv, Q. Li, T. Men, C. Zhao, D. Xiao, J. Wu, K. Wang, J. F. Li, Y. Gu, J. Zhu, and S. J. Pennycook, *Energy Environ. Sci.* **10**, 528 (2017).
- [17] H. J. Trodahl, N. Klein, D. Damjanovic, N. Setter, B. Ludbrook, D. Rytz, and M. Kuball, *Appl. Phys. Lett.* **93**, 262901 (2008).
- [18] S. Klauer and M. Wöhlecke, *Phys. Rev. Lett.* **68**, 3212 (1992).
- [19] N. Waesermann, B. Mihailova, B. J. Maier, C. Paulmann, M. Gospodinov, V. Marinova, and U. Bismayer, *Phys. Rev. B* **83**, 214104 (2011).
- [20] W. Zhu, J. Zhu, M. Wang, B. Zhu, X. Zhu, and G. Pezzottia, *J. Raman Spectrosc.* **43**, 1320 (2012).
- [21] S. Sanna, S. Neufeld, M. Rüsing, G. Berth, A. Zrenner, and W. G. Schmidt, *Phys. Rev. B* **91**, 224302 (2015).
- [22] S. Tsukada, Y. Fujii, Y. Yoneda, H. Moriwake, A. Konishi, and Y. Akishige, *Phys. Rev. B* **97**, 024116 (2018).
- [23] C. Banwell and E. McCash, *Fundamentals of Molecular Spectroscopy* (McGraw-Hill, New York, 1994).
- [24] L. Rayleigh, *Philos. Mag.* **274**, 447, XLI (1871).
- [25] J. Zhang, W.-Y. Tong, J. Zhu, J. Xu, Z. Duan, L. Xu, Z. Hu, C.-G. Duan, X. Meng, Z. Zhu, and J. Chu, *Phys. Rev. B* **91**, 085201 (2015).
- [26] F. Wu, B. Yang, E. Sun, R. Zhang, D. Xu, J. Zhou, and W. Cao, *J. Alloys Compd.* **551**, 98 (2013).
- [27] J. Zhu, K. Jiang, G. Xu, Z. Hu, Y. Li, Z. Zhu, and J. Chu, *J. Appl. Phys.* **114**, 153508 (2013).
- [28] C. Chen, H. Deng, X. Li, H. Zhang, T. Huang, D. Lin, S. Wang, X. Zhao, Z. Hu, and H. Luo, *Appl. Phys. Lett.* **105**, 102909 (2014).
- [29] G. de la Flor, T. Malcherek, S. Gorfman, and B. Mihailova, *Phys. Rev. B* **96**, 214102 (2017).
- [30] T. Shigenari, K. Abe, T. Takemoto, O. Sanaka, T. Akaike, Y. Sakai, R. Wang, and M. Itoh, *Phys. Rev. B* **74**, 174121 (2006).
- [31] Y. Saito, H. Takao, T. Tani, T. Nonoyama, K. Takatori, T. Homma, T. Nagaya, and M. Nakamura, *Nature (London)* **432**, 84 (2004).
- [32] E. Cross, *Nature (London)* **432**, 24 (2004).
- [33] J. Hao, W. Li, J. Zhai, and H. Chen, *Mater. Sci. Eng., R* **135**, 1 (2019).
- [34] K. Wang, F. Yao, W. Jo, D. Gobeljic, V. V. Shvartsman, D. C. Lupascu, J. Li, and J. Rödel, *Adv. Funct. Mater.* **23**, 4079 (2013).
- [35] S. Jabarov, V. Aliyeva, T. Mammadov, A. Mammadov, S. Kichanov, L. Dubrovinsky, S. Babayev, E. Pashayeva, and N. Dang, *Mater. Sci.-Pol.* **36**, 203 (2018).
- [36] E. Capitaine *et al.*, *Phys. Rev. B* **94**, 245136 (2016).
- [37] M. Chen, Y. Wang, C. Huang, W. Wang, and H. Chui, *J. Phys. D: Appl. Phys.* **51**, 385303 (2018).
- [38] M. Kim, X. M. Chen, Y. I. Joe, E. Fradkin, P. Abbamonte, and S. L. Cooper, *Phys. Rev. Lett.* **104**, 136402 (2010).
- [39] R. Zallen and E. M. Conwell, *Solid State Commun.* **31**, 557 (1979).
- [40] R. Zallen and M. L. Slade, *Phys. Rev. B* **18**, 5775 (1978).
- [41] M. Deshpande, S. Bhatt, V. Sathe, R. Rao, and S. Chaki, *Physica B* **433**, 72 (2014).
- [42] H. Yurtseven and D. Kavruk, *J. Mol. Struct.* **924**, 544 (2009).
- [43] H. Rho, S. Cooper, S. Nakatsuji, and Y. Maeno, *J. Magn. Magn. Mater.* **310**, e266 (2007).
- [44] D. Wolverson, in *Characterization of Semiconductor Heterostructures and Nanostructures*, edited by C. Lamberti (Elsevier, Amsterdam, 2008), pp. 249–288.
- [45] J. Grindlay, *An Introduction to the Phenomenological Theory of Ferroelectricity* (Pergamon, Oxford, 1970).
- [46] R. Frech and J. C. Decius, *J. Chem. Phys.* **51**, 5315 (1969).
- [47] S. Porto, Porto's notation, Bilbao crystallographic, Raman scattering, <http://www.cryst.ehu.es/cgi-bin/cryst/programs/nph-doc-raman>.